Snap-through behaviour of gradient-stiffness metastructures

PME, TU Delft, the Netherlands

Deime Schoneveld 4395980 | Berry Vermin 4443012 | Julius Keur 4342879 | Quinten de Wit 4452771

***Abstract*—Metastructures form a versatile family of mechanical structures with unique properties. This paper discusses metastructures consisting of bistable unit cells and their snap-through behaviour. The main scope is on changing structural stable-state properties of gradient-stiffness metastructures. Numerical and FEA models, as well as a physical test setup are made. The FEA model gives an accurate prediction of the force-displacement curve of a single unit cell, while the numerical metastructure model represents the *F-d* curve characteristics for metastructures, for different actuation points. Furthermore, the metastructure model is expanded to predict the behaviour of structures that are scaled versions of the physical test samples.**

***Keywords*—Bistability, Metastructure, Snap-Buckling, Stiffness, Unit Cell**

I. Introduction

Metastructures are structures where the properties rely not solely on material properties, but also on structure design and configuration [1]. Within the scope of metastructures, this paper focuses on metastructures that exist of several bistable unit cells. These unit cells contain an internal spring that exhibits snap-through behaviour when a force is applied perpendicular to the spring. Combining these unit cells in a structure will lead to multistable behaviour.

Series-orientation (stacking horizontal layers) can lead to multistable behaviour, but the resulting force-displacement characteristics of the structure between two stable states do not differ much from individual unit cells. Furthermore, the order of snap-through behaviour of the different layers cannot be predicted [2]. This order can both be predicted and even modified by changing the properties of the unit cells per layer [1]. Changing the stiffness per horizontal layer results in a predictable order of snap-through behaviour, but this does not change the type of multistability of the structure. Different stable states are ones where the layers of unit cells differ only in being fully collapsed or not. This means the multistability of the structure is unidirectional, so only in the direction of the applied force.

From [3] it became clear that a parallel-configuration of unit cells also has multistable behaviour, but not unidirectional like in [1] and [2]. Instead, this physical model could rotate as well, and showed that multistability of the metastructure depends on the location of actuation on the structure.

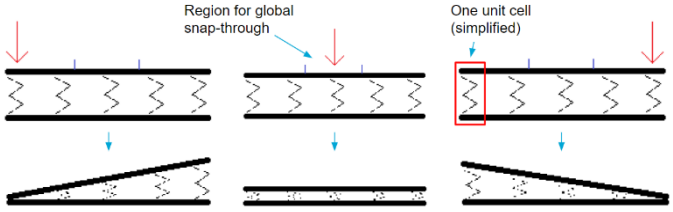

Fig 1: Different snap-through behaviour under force

When considering a one-dimensional metastructure of identical bistable unit cells, placed in parallel orientation, it is expected that one of three stable outcomes are possible when subjected to a force (see figure 1).

This figure also shows that it is expected that actuation within a certain region results in global snap-through behaviour. When adjusting the individual stiffness of unit cells, this region is expected to change position and size. These expectations result in the following research question:

How does variation of stiffnesses in a one-dimensional metastructure, consisting of bistable unit cells, influence the range of actuation points that trigger global snap-through behaviour of the structure?

A test setup is made to test both the individual cells and one-dimensional metastructures. A design of a unit cell as well as a jig for several cells in a larger structure is made, while allowing a variation in stiffness. Numerical and FEA models are used to predict the behaviour of unit cells, as well as metastructures that consist of these cells. To validate these models, physical tests are performed. The models are used to answer the research question for versatile configurations of the metastructure design, even for structures that are larger than those that were tested physically.

II. Design and Experimental Setup

In this chapter, a short overview of the design specifications and testing methodology is given.

A. Design

A CAD model (figure 2) is built to make a setup for testing in a tensile tester. The design comprises five unit cells. Each unit cell consists of a 3D printed frame and two interconnected spring steel crosses, which are constrained parallel to the xy-plane by six bolts. These crosses form the beams that give the unit cell its bistable properties. Constraining the centres of the crosses to the bottom plate prevents the bistable beams to buckle in the second mode, hence it only buckles in first and third mode (see figure 3). Since the five unit cells are positioned parallel to each other, the model forms a one-dimensional structure. To prohibit rotation of the structure around the x-axis, the structure consists of two rows of springs instead of a single row.

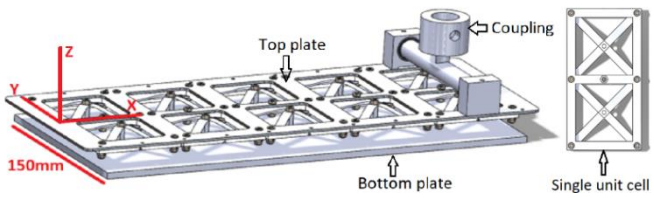

Fig 2: CAD model of the design

The cells are rigidly connected to a stiff top plate, which is attached to the actuator coupling that forms the connection between the test sample and the tensile testing machine. The actuator coupling uses two ball bearings to allow rotation of the sample with respect to the tensile tester machine. This rotation

causes a small translation in the x-direction, but its influence is deemed negligible.

Variation of unit cell stiffness is achieved by using 0.05 mm, 0.1 mm and 0.2 mm thick spring steel beams (alloy 1.4310) with stiffness k_1, k_2 and k_3 respectively. All the frames are 3D printed PLA with 20% infill. All other components are made of aluminium.

B. Methodology

As soon as the tensile testing machine has been calibrated such that it gives repeatable results, each test is done three times. The average from these three tests is used to get a force-displacement (*F-d*) curve. First, each unit cell is tested separately. Then *F-d* curves are obtained for three reference structures of five unit cells with uniform stiffness: k_1, k_2 and k_3. Finally, several structures with gradient stiffness are tested. When the structures are being tested, the actuation point is varied.

III. Numerical Models

This chapter explains how the different models are set up.

A. Analytical Model of a single cell

The *F-d* curve of a single unit cell is determined by an approximation of the contribution of the different mode shapes. The model that is used contains the Euler-Bernoulli equation for a beam as described in [4] and [5]. The deflection of the beam is given by a summation of buckling modes 1 and 3 for a clamped-clamped beam, which is given by:

$$y(x) = a_1 * \left(1 - \cos\left(\frac{2 * \pi * x}{L}\right)\right) + a_3 * \left(1 - \cos\left(\frac{4 * \pi * x}{L}\right)\right) \quad (1)$$

Where $y(x)$ is the deflection of the beam at distance x from one end of the beam and L is the compressed beam length. The first buckling mode, which is represented by coefficient a_1, is used for the static stability of the beam and defines the starting position. The third buckling mode, which is represented by coefficient a_3, is used to transfer the beam from one stable state to the other. It lowers the energy needed for the displacement of the beam through vertical motion.

To solve for a_1 and a_3, the energy equations for a compressed beam must be taken into account. These equations consist of the externally applied energy, as well as the internal energy of the system. The bending energy is approximated by:

$$U_b = \frac{E * I_x}{2} * \int_0^L y''(x)^2 \, dx \quad (2)$$

Where E is the Young's modulus and I_x is the area moment of inertia. The compression energy is calculated by using Hooke's law which is given by:

$$U_c = \frac{A * E * \left[2 * (L - L_0) + \int_0^L y'(x)^2 dx\right]^2}{8 * L_0^2} \quad (3)$$

Here A is the cross-section area of the beam and L_0 is the initial beam length. The energy resulting from the external force is the opposite of the work, which results in:

$$U_f = -F * y(x) \quad (4)$$

F is the force applied perpendicular to the beam. The total energy of the system is the sum of all these energies:

$$U_{tot} = U_b + U_c + U_f \quad (5)$$

The next step is to obtain the equilibrium solution for the system by using the minimal energy of equation 5. That is when the following two equations are solved simultaneously for a given force:

$$\left\{\frac{\partial U_{tot}}{\partial a_1} = 0, \frac{\partial U_{tot}}{\partial a_3} = 0\right\} \quad (6)$$

This system has two third order polynomial equations and multiple solutions, hence it is solved by using numerical solvers [6] and [7]. This results in 5 different combinations for a_1 and a_2. Two of these solutions are stable (S_1, S_2), one is unstable (U) and two are undefined (D_1, D_2) as shown in figure 3. Therefore, the right solutions need to be filtered out by inserting these values into equation 1 and plotting them against the force that they are solved for. The result is shown in figure 5 where the black line represents the theoretical model.

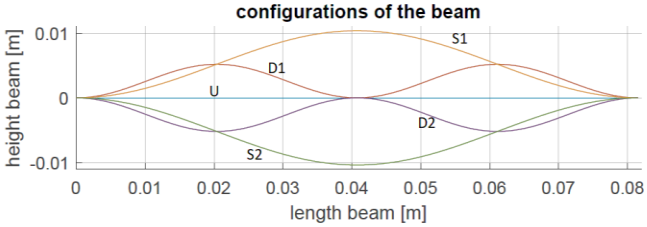

Fig. 3: Equilibrium modes for a buckled beam. The lines D_1 and D_2 represent the third mode buckling and lines S_1 and S_2 represent the first mode buckling.

B. FEM Model of a single cell

To validate the numerical model, a finite element method solver has been used [8]. The same parameters are used in the solver as in the theoretical model. The mesh is tetrahedral at the curved edges of the beam and hexagonal on the non-curved geometry, it is also a minimum of two elements thick. This all is used to reduce solver time and increase the accuracy of the result. The solution is obtained using a 3-step static study and the nonlinear solver. The first step introduces an instability, the second step introduces the compression force and the third step presses the beam from one stable state to the other. In the third step a damping factor of 10^{-4} is applied, as the system would otherwise vibrate and become unstable.

C. Metastructure Model

The numerical model for different metastructures is made with the use of numerical solvers [6] and [7]. It is based on a model for n number of unit cells, which are connected to an infinitely stiff top plate (see figure 4). The stiffnesses of the unit cells are taken from the test data, but with the assumptions that it behaves linearly between the maximum and minimum values of the curve (see figure 5). To calculate the displacement of each cell, a static force- and moment-equilibrium and goniometric formulas (7-9) are used. F_{app} is the applied force, y_i is the displacement of cell i, k_i is the stiffness of cell i, x_i is the distance between cell i and the actuation point and y_p is the displacement of the actuation point. The input for the model is the point of actuation and the given configuration. The output is an *F-d* curve.

$$\sum_{i=1}^{n} y_i k_i - F_{app} = 0 \quad (7)$$

$$\sum_{i=1}^{n} y_i k_i x_i = 0 \quad (8)$$

$$y_i = y_p + x_i \frac{y_1 - y_p}{x_1} \quad (9)$$

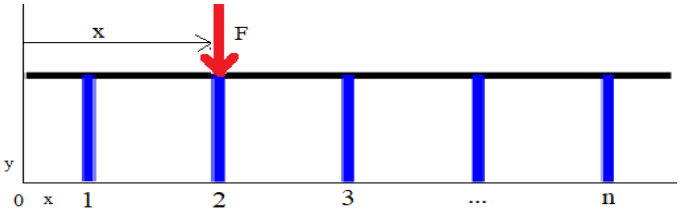

Fig 4: A graphical overview of the model

IV. Results

A. Single unit cell

All the results of the simulations are for a beam with length L = 81.5 mm, uncompressed length L_0 = 84.76 mm, width b = 10 mm, thickness t = 0.01 mm and elastic modulus E = 185 GPa. The system is investigated at an actuation location at the centre of the beam (L/2) in a clamped-clamped position where the second mode buckling is constrained. The results are shown in figure 5.

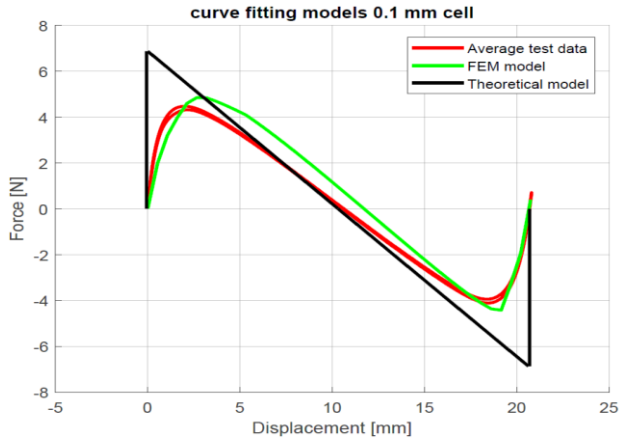

Fig 5: Simulation results with the experimental results

B. Metastructure

Figures 6 and 7 display the *F-d* curves of the test results and the numerical model. The tested metastructure has a uniform distribution of cells with stiffness k_2 and one cell on cell position 1 (see figure 4) with a stiffness of k_3. In figure 6 the actuation point is on the first unit cell and in figure 7 it is on the second cell. The red curves represent the mean of three tests and the black curves represent the numerical model. Graphical representations of the metastructures position, as calculated by the numerical model, are shown next to the graphs. At point 3 in figure 7 the structure is observed to be in an angled stable state. Tests with application points at positions right from the second unit cell show the presence of an angled stable state, just like figure 7.

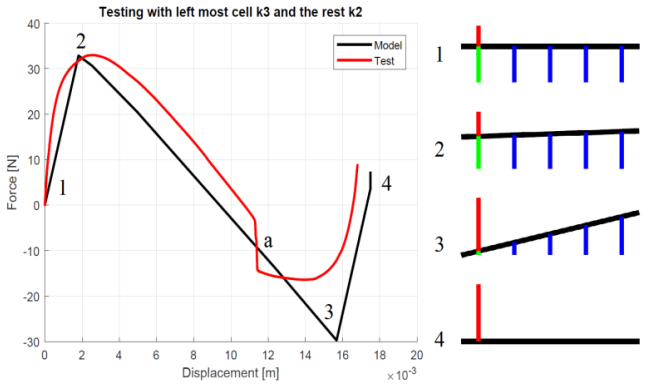

Fig 6: F-d curve of the sample with actuation on first cell (the green line is the unit cell with stiffness k_3 and the blue lines are unit cells with stiffness k_2)

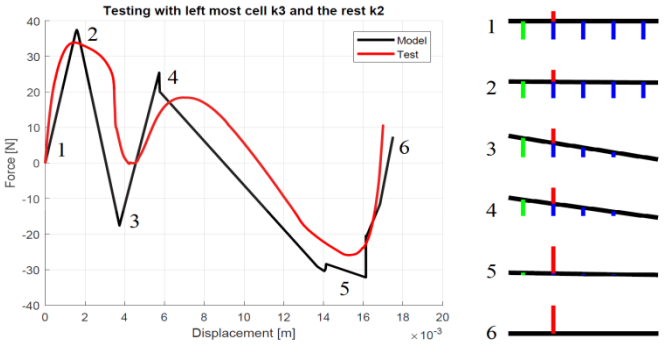

Fig 7: F-d curve of the sample with actuation on second cell

V. Discussion

In this chapter the results will be discussed. First, aspects that may have influenced the results will be reviewed, after which results for the single-cell model and metastructure model will be discussed.

A. Manufacturing errors

A heavy influencer of the results was the large variation in *F-d* curves between cells of the same stiffness, this was mostly caused by manufacturing errors. The laser cutter did not cut at a high enough accuracy, resulting in holes which were offset up to 2 mm, beam widths that varied between 6 mm and 8 mm, while the width of the beam should have been 7 mm. The characteristics of the system are mostly dependent on the initial beam length, which is determined by the locations of the holes. This, along with other influences, resulted in the following means (μ) and standard deviations (σ) between the *F-d* curves of unit cells with stiffness k_2:

	μ	σ
Maximum Force	0.615 N	0.0293 N
Minimum Force	-0.5978 N	0.0608 N
Actuation Distance	20.3 mm	2.0 mm

Table 1: Means and standard deviations from the tested unit cells with stiffness k_2

This variation in unit cell characteristics has a large negative influence on the applicability of the reference structures (see paragraph II.B), which is why these are not represented in the results.

B. Single cell models

Figure 5 shows that the FEA model has a high degree of accuracy for the *F-d* curve and the theoretical model has a large error compared to the test results. The theoretical model is a linear approximation of the curve. This is due to the fact that the ratio of total displacement over thickness ($Q = h/t$) is very large, as described in [9]. With our parameters the value for Q is 208, which results in the linear behaviour of the *F-d* curve. As the theoretical model describes how the system works, it does not include the irregularities like the fillets in the middle of the beam and the holes on the outer edge. The FEA simulation gives better results for the beam.

C. Metastructure model

Figure 6 shows that the numerical model and the test data are correlated, but show some differences. These differences can be attributed to the assumption of linearity in the model and the imperfections in production. Furthermore, the graphical representations 1, 2 and 4 in figure 6 were also observed during testing. At point ‘a’ in figure 7 the red curve shows a sudden

steep slope. This is caused by the free motion of the plate with respect to the location of the actuation point, as this point is constrained in the z-direction by the machine. The point where the actuation point is attached cannot collapse, but the other end is free to move and can thus collapse. This effect is amplified by the weight of the top plate and the momentum of the structure at that instance. Therefore, the graphical representation at point 3 is not representative for what was observed during the tests.

In figure 7, the numerical model is less representative for the test data compared to figure 6, but they are still correlated. The differences between the model and the test are caused by free motion of a part of the structure, as already mentioned. This leads to movement of the structure, which is not taken into account in the numerical model. At position 3 the structure has an angled stable state, which was also observed during testing. At that point a force needs to be added to the system to get the system to another position. During hand testing it was not possible to achieve this result, because of human errors. Also, when pushing by hand there is a dynamic actuation, but during the test any input from the machine is quasi-static. Furthermore, it was observed that actuation on the side where unit cells have stiffness k_2 results in an angled stable state of the structure.

When these results are compared to a metastructure with uniform stiffness, as shown in [3], there is a change in the region of actuation points that result in global snap-through behaviour. Actuation on the leftmost (first) unit cell of the gradient-stiffness structure resulted in global snap-through behaviour and actuation on the second unit cell and further to the right resulted in an angled stable state. Global snap-through behaviour of a metastructure with uniform stiffness is achieved by actuation in the middle of the structure. An angled stable state is the result of actuation on the sides of the structure [3].

D. Scaling

Since the numerical model and test data are correlated, it is interesting to see how a scaled metastructure would behave. In figure 8 the black line shows the *F-d* curve used in figure 7 and the green line represents a 10x2 metastructure with scaled characteristics; the first two cells have stiffness k_3, the other eight have stiffness k_2. The actuation point is between cells 3 and 4, as it is scaled as well. The blue line is a 15x2 metastructure, which is three times the size of the 5x2 structure. Figure 8 shows that the two larger structures follow the same trend line as the 5x2 structure at a displacement of around 4 mm. For the 5x2 structure, this indicated that there was an angled stable state, so it is likely that this is also the case for the larger structures.

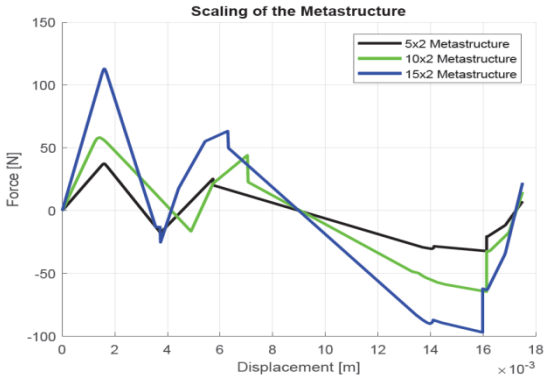

Fig 8: F-d curve of a scaled metastructure

VI. Conclusion

The research goal was to find out what happens to the snap-through behaviour when there are different stiffnesses in a metastructure. After all the tests and the results from the model it can be concluded that, with a variation in stiffness per unit cell, the actuation region where the metastructure will have a certain stable state (global or angled) will change. The position of moment equilibrium determines each regions location. Placing a stiff cell on the edge of a structure allows for a global snap-through actuation point that is closer to this edge.

Furthermore, it can be shown that the FEA model results in a more accurate prediction of mechanical behaviour of single unit cells compared to the numerical model, although this provides less insight in the working principles of snap-buckling behaviour. The numerical metastructure model predicts trends in the structure's behaviour, but cannot provide a precise result.

VII. Future Recommendations

Right now, the numerical metastructure model is a linear approximation, which only gives an indication of how a structure may behave. A first step might be to make a nonlinear model and take into account dynamical behaviour. While the numerical single cell model gives insight in how the system works, it does not provide accurate results, hence solely using an FEA model may provide better results, as well as a stress distribution. This method, however, provides little insight in the actual working principles of snap-buckling. Finally, if a new numerical model is built, it should be built to be easily scalable, so scaled structures can be evaluated.

Acknowledgements

We would like to thank our supervisors Marcel Tichem and Yong Zhang for guiding us in our research and Bradley But for his help with manufacturing.

References

[1] K. Che, C. Yuan, J. Wu, H. Jerry Qi and J. Meaud, "Three-Dimensional-Printed Multistable Mechanical Metamaterials With a Deterministic Deformation Sequence," *Journal of Applied Mechanics*, vol. 84, no. 1, p. 10, 10 September 2017.

[2] A. Rafsanjani, A. Akbarzadeh and D. Pasini, "Snapping Mechanical Metamaterials under Tension," 18 December 2016. [Online]. Available: https://arxiv.org/abs/1612.05987. [Accessed 3 November 2018].

[3] Y. Zhang, Q. Wang, M. Tichem and A. van Keulen, "Design and characterization of multi-stable mechanical structures with tilting behaviour," *In preparation.*

[4] P. Cazottes, A. Fernandes, J. Pouget and M. Hafez, "Bistable Buckled Beam: Modeling of Actuating Force and Experimental Validations," *Journal of Mechanical Design*, vol. 131, no. 10, p. 10, 2 September 2009.

[5] J. Cleary and H.-J. Su, "Modeling and Experimental Validation ofActuating a Bistable Buckled Beam Via Moment Input," *Journal of Applied Mechanics*, vol. 82, no. 5, p. 7, 31 March 2015.

[6] "Maple," 1 November 2018. [Online]. Available: https://www.maplesoft.com/products/Maple/.

[7] "Matlab," Mathworks, 1 november 2018. [Online]. Available: https://nl.mathworks.com/.

[8] "Simulia Abaqus," 2 December 2018. [Online]. Available: https://www.simuleon.com/simulia-abaqus.

[9] J. Qiu, J. H. Lang and A. H. Slocum, "A Curved-Beam Bistable Mechanism," *Journal of Microelectromechanical Systems*, vol. 13, no. 2, pp. 137-146, 2004.